A study of the change in the wave field due to the presence of wave energy converters

Ola Kalén

Degree project for Master of Science (Two Years) in
Earth Sciences
30 hec

Department of Earth Sciences
University of Gothenburg
2010 B593

Faculty of Science

UNIVERSITY OF GOTHENBURG

UNIVERSITY OF GOTHENBURG
Department of Earth Sciences
Geovetarcentrum/Earth Science Centre

A study of the change in the wave field due to the presence of wave energy converters

Ola Kalén

ISSN 1400-3821

B593
Master of Science (Two Years) thesis
Göteborg 2010

Mailing address
Geovetarcentrum
S 405 30 Göteborg

Address
Geovetarcentrum
Guldhedsgatan 5A

Telephone
031-786 19 56

Telefax
031-786 19 86

Geovetarcentrum
Göteborg University
S-405 30 Göteborg
SWEDEN

Abstract

This paper investigates the change of wave field characteristics due to the presence of the oscillating buoys of wave energy converters in the ocean. A general theory for devices of the point absorber type, whose dimensions are much smaller than the incident wavelength, is presented. To simplify the process of accounting for wave and body interactions, a small body approximation is used, in which the diffracted wave field that arises when the incident wave is scattered on a body moving with the same amplitude and phase as the wave, is neglected. The formulation for the radiated wave, which is due to the vertical displacement of the buoy relative to the wave surface, is expressed with a plane wave approximation.

The theory is applied to a wave power concept called the Lysekil project, developed at Uppsala University. Model simulations using data from this system were obtained with the boundary element solver WAMIT. With the use of model output, the amplitude of the radiated wave and the phase shift between the incident and radiated wave can be approximated. This enables calculations of total wave amplitudes at arbitrary positions due to interference of the incident wave and sum of radiated waves from multiple buoys. These findings can be used both to assess environmental impact as well as to enhance the performance of wave farms. The dependence of the amplitude on the distance between devices is shown for arrays of devices in regular grids. The difference between low and high values at varying distance could be considerable. Applied to a location for a future wave farm on the Swedish west coast, the difference may be significant in terms of energy content available for absorption for a typical incident frequency.

Contents

1. Nomenclature 2
2. Introduction 3
3. Theory 3
3.1 Linear wave theory 3
3.2 Interaction between waves and bodies 5
3.2.1 Diffracted and radiated wave fields 6
3.2.2 Energy extraction and wave field energy fluxes 8
3.2.3 Flux of energy: an elongated body 9
3.2.4 Circular waves 11
3.2.5 Flux of energy: a point absorber 13
3.2.6 Wave amplitudes for an array of point absorbers 15
3.2.7 Relation between buoy movements and the radiated wave field 17
4. Methods 18
5. Results 20
5.1 Validity of the small body approximation 20
5.2 Phase shift and amplitude of the radiated wave 20
5.3 Wave field for two point absorbers 22
5.4 Wave field for arrays of point absorbers 23
6. Discussion and conclusions 27
7. Acknowledgments 28
8. References 29

1. Nomenclature

Symbol	Quantity	S I Unit
u	velocity	ms^{-1}
m	mass	kg
Φ	velocity potential	m^2s^{-1}
t	time	s
g	acceleration of gravity	ms^{-2}
p	pressure	Nm^{-2}
ρ	density of seawater	kgm^{-3}
ν	kinematic viscosity	m^2s^{-1}
h	water depth	m
H	wave height	m
k	wave number	m^{-1}
λ	wave length	m
ω	angular frequency	$rads^{-1}$
T	wave period	s
c	phase speed	ms^{-1}
c_g	group speed	ms^{-1}
η	surface elevation of wave	m
η_{ro}	amplitude of radiated wave	m
r	distance from origin or between bodies	m
φ	phase shift	rad
E_p	potential energy density per unit area	Jm^{-2}
E_k	kinetic energy density per unit area	Jm^{-2}
J	energy flux per meter wave front	Wm^{-1}
P	power	W
z	vertical position	m
$\hat{H}$	complex valued transfer function	-
F	force	N
γ	damping coefficient	Nsm^{-1}
k_s	spring constant	Nm^{-1}

2. Introduction

This paper is a continuation of sorts to my bachelor thesis (Kalén, 2009), which probed what possible effects the reduction of energy in the wave field due to wave energy converters could have on the bottom friction. The system of conversion of wave energy to electricity applied in that study was the wave power concept called the Lysekil project (Leijon et al., 2008 and Engström, 2009), developed by the division for Electricity within the Swedish Centre for Renewable electric energy at Uppsala University. The wave energy converter (WEC) of the Lysekil project consists of a direct driven linear generator, located on the seabed, with a semi-submerged buoy at the surface that absorbs the wave energy. The results using data from this system was then applied to a future wave energy farm to be located outside of Smögen on the Swedish west coast, planned by the Swedish company Seabased. In the present paper I again had the opportunity to cooperate with Jens Engström at Uppsala University and share his knowledge and experience from the Lysekil project. The subject this time also regards the impact of WECs but the question was how the presence of the oscillating devices could influence the characteristics of the wave field.

Many efforts in design and optimization of wave energy devices have their base in the hydrodynamic forces subject on the devices, found through the solution of an equation of motion for the whole system. This is often carried out numerically with the use of commercial boundary element codes. In these circumstances, the properties of the wave field itself are often not considered. The aim of this paper is to gain understanding in how the wave field is changed by the energy converters. If this change is significant, it could also possibly be an effect to include when optimizing the performance of systems for energy conversion. In addition the results and methods would be relevant for an environmental study concerning changes in the marine or benthic environment caused by a wave energy farm. In (Kalén, 2009) the rate of reduction of energy flux due to WECs could only be vaguely approximated. The tools presented in this study would enhance the description of this effect.

3. Theory

3.1 Linear wave theory

Airy wave theory or linear wave theory can be used to express the propagation of surface gravity waves in a homogenous fluid. Surface gravity waves created by the wind are the type of waves that are relevant to the systems of conversion of wave energy to electricity described in this paper. Other types of ocean waves such as tidal waves and internal waves are not considered here.

The governing equations in the linear wave theory are the continuity equation:

$$\frac{\partial \rho}{\partial t} + \nabla \cdot (\rho \mathbb{u}) = 0 \qquad (1)$$

and the Navier-Stokes equation

$$\frac{\partial \mathbb{u}}{\partial t} + \mathbb{u} \cdot (\nabla \mathbb{u}) = -\frac{1}{\rho}\nabla P + \nu \nabla^2 \mathbb{u} + \frac{1}{\rho}\mathbb{f} \tag{2}$$

where ρ is the density, $\mathbb{u}$ the velocity vector of a fluid element, P the pressure, $\mathbb{f}$ the external forces of the fluid element and ν the kinematic viscosity. Consider surface gravity waves of constant form and period T propagating in the x-direction in an ocean of uniform depth h. The wave-height H is small compared to the wavelength λ. The linearization of the governing equations and the introduction of a velocity potential Φ yields the Laplace equation

$$\nabla^2 \phi = 0 \tag{3}$$

The solution to (3), subject to three linearized boundary conditions, is a well known problem. More details can be found in (Kundu, 2008).

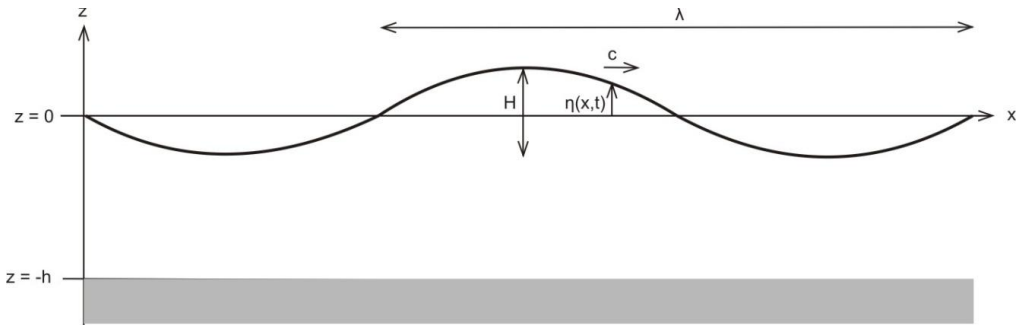

Figure 1. *Surface wave definitions*

If the surface elevation of the wave is assumed to be of the form

$$\eta(x,t) = \frac{H}{2}\cos(kx - \omega t) \tag{4}$$

where H is the wave height, k = 2π/λ is the wave number and ω = 2πf = 2π/T is the angular frequency, the solution to the Laplace equation (3) will give the velocity component u for the fluid element

$$u = \frac{H\omega}{2}\frac{\cosh\ k(z+h)}{\sinh\ kh}\cos(kx - \omega t) \tag{5}$$

The dispersion relation is given by

$$\omega^2 = gk\ \tanh kh \tag{6}$$

The phase speed of the waveform, c = ω/k then yields

$$c = \sqrt{\frac{g}{k}\tanh kh} = \sqrt{\frac{g\lambda}{2\pi}\tanh\frac{2\pi h}{\lambda}} \tag{7}$$

It can be shown that the energy of a wave does not travel with the phase speed, but with the speed of the whole wave packet, the group speed, which is equal to

$$c_g = \frac{c}{2}\left(1 + \frac{2kh}{\sinh\ 2kh}\right) \tag{8}$$

Since sinh kh tends to infinity when kh >>1, the group speed for deep-water waves can be approximated to

$$c_g = \frac{c}{2} \tag{9}$$

The energy content of surface gravity waves consists mainly of mechanical energy, normally measured in mean energy density per unit horizontal area. It is the sum of the potential energy due to the displacement of the water surface and the kinetic energy due to the motion of the fluid particles. In this context, the effects of surface tension and dissipation are negligible.

The total mean energy density per unit area is

$$E = E_p + E_k = \rho g \langle \eta^2 \rangle = \frac{1}{8}\rho g H^2 \tag{10}$$

where the variance of the sea surface displacement is denoted $\langle \eta^2 \rangle$. The transmission of energy due to wave motion is the pressure work done by the fluid. The mean energy flux per unit length of crest is the mean value of the energy that is transmitted through a vertical section, integrated over the whole depth:

$$J = \langle \int_{-h}^{o} pu\, dz \rangle = \langle \int_{-h}^{0} p'u\, dz \rangle - \rho g \int_{-h}^{0} \langle u \rangle z\, dz = \langle \int_{-h}^{o} p'u\, dz \rangle \tag{11}$$

where the pressure p is expressed as a sum of a perturbation pressure p´ and a background pressure -ρgz. The perturbation pressure can be expressed as

$$p' = \frac{\rho H \omega^2}{2k} \frac{\cosh\ k(z+h)}{\sinh\ kh} \cos(kx - \omega t) \tag{12}$$

Substitution of (12) as well as the velocity component (5) into equation (11) then yields

$$J = \frac{1}{8}\rho g H^2 \left[\frac{c}{2}\left(1 + \frac{2kh}{\sinh\ 2kh}\right)\right] = E\ c_g \tag{13}$$

Using the deep-water approximation (9) to apply the relation $c_g = g/2\omega$, the mean energy flux is found to be

$$J = \frac{1}{8}\rho g H^2 \frac{g}{2\omega} = \frac{\rho g^2 T H^2}{32\pi} \tag{14}$$

3.2 Interaction between waves and bodies

The theory for the absorption of wave energy described in this paper is valid for wave-activated bodies moving relative to a fixed reference at the seabed. The oscillating motions of the body are induced by the incident waves. The theory does not apply to large devices with dimensions of the same magnitude as the incident wave, such as the Pelamis (Caracas, 2003). Other concepts for wave energy extraction such as oscillating water columns or overtopping devices are not

considered here. Examples of such systems are the Limpet (Falcão, 2000) and the Wave Dragon (Kofoed et al., 2006). For a thorough outline of contemporary systems, see (Cruz, 2008).

3.2.1 Diffracted and radiated wave fields

A rigid body subject to incident waves moves in response to the force of the waves in six degrees of freedom, defined as surge, sway, heave, roll, pitch and yaw, as shown in fig. 2.

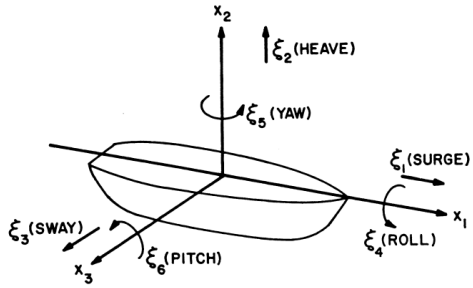

Figure 2. *Body motions in six degrees of freedom. Image from (Newman, 1977).*

In this paper, the body motions are restricted to heave only. When the term incident wave is used, a propagating wave which can be described by (4) is meant. To further clarify notation, this is not equivalent to a wave incident at a certain position, which can mean any type of wave that is propagating towards this position. The amplitude of the wave is the maximal value of vertical displacement experienced during a period T, whereas the surface elevation of the wave, or wave elevation, is an instantaneous value. The presence of an oscillating body in an incident wave field results in a diffracted and radiated wave field. The diffracted wave field arises when the incident wave field is scattered on the body, which follows the motion of the incoming waves. The amplitude of this disturbance is proportional to the dimensions of the body. Usually the body is not exactly following the motions of the wave, but oscillates with a somewhat different amplitude and phase. The displacement of the body relative to the wave surface causes a radiated wave field. An illustration of this is shown in fig. 3.

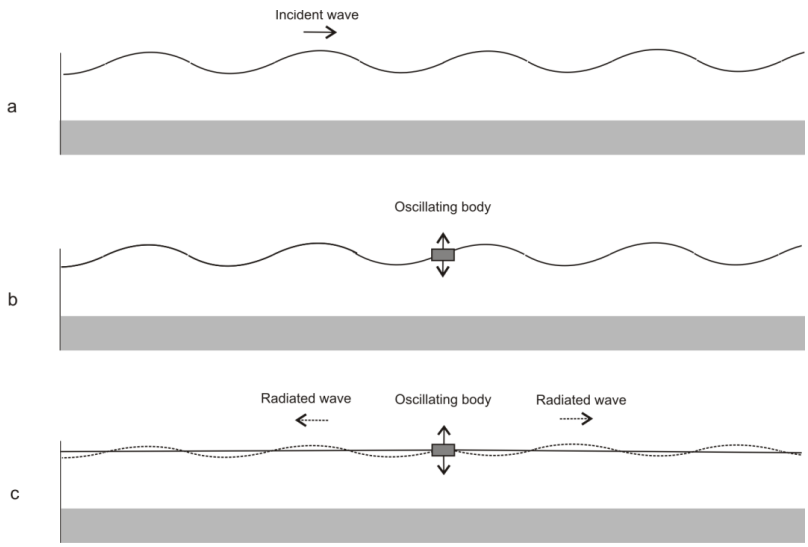

Figure 3. *Wave fields due to oscillations. Panel a shows an undisturbed incident wave. Panel b shows a body oscillating with the same frequency, amplitude and phase as the incident wave. Panel c shows an oscillating body, which creates a radiated wave. For a body that oscillates with a different amplitude or phase than the incident wave, the resulting wave field will be superposition of b and c.*

Now the above discussion will be defined in terms of mathematical expressions. For clarity and ease of calculations, it is advantageous to use a complex notation. By the assumed linearity and harmonic oscillation of the wave motions, the time dependence may be extracted. A complex wave elevation $\hat{\eta}$ can then be defined, where

$$\eta = Re\{\hat{\eta}e^{i\omega t}\} \tag{15}$$

is the time dependent real wave elevation. The total wave field due to the incident waves and the presence and oscillations of the body in the incident wave field can, by the linearity of the problem, be decomposed as

$$\hat{\eta}_{tot} = \hat{\eta}_i + \hat{\eta}_d + \hat{\eta}_r \tag{16}$$

where all quantities now are frequency dependent. Note that this decomposition is different from the one often used for describing wave and body interactions via the hydrodynamic forces, as in the theory behind the numerical solver WAMIT, which is described in chapter 4. The diffracted wave field $\hat{\eta}_d$ arises when incident waves with elevation $\hat{\eta}_i = \frac{H}{2}e^{-ikx}$ are scattered on a body oscillating with the same frequency, amplitude and phase as the wave. The surface elevation of the radiated wave due to the displacement of the body relative to the incident wave is denoted $\hat{\eta}_r$. The vertical displacement z of the body from its equilibrium position can be described by

$$\hat{z} = \hat{H}\hat{\eta}_i \tag{17}$$

where $\hat{H}(\omega)$ is a complex transfer function describing the amplitude response $\hat{z}$ of the body to the incident wave. The displacement of the body relative to the wave is also an oscillation with the complex amplitude

$$\hat{z} - \hat{\eta}_i = (\hat{H} - 1)\hat{\eta}_i \neq 0 \tag{18}$$

The radiated wave elevation is proportional to the magnitude of the amplitude difference (18).

3.2.2 Energy extraction and wave field energy fluxes

For the body to be able to absorb energy there must be a reduction of the energy in the waves that are passing the body or are being reflected from it. On the leeside of the body, energy levels will be lower than on the side facing the incident waves. The wave that is radiated due to the oscillatory motion of the device must reduce or cancel out the other waves, i.e. interfere destructively. This can be realized if the generated waves oppose the incident waves. For a wave to be generated, the frequency, amplitude or phase of the body motion must be different from those of the incident wave. If the body oscillates with the same frequency, amplitude and phase as the incident wave, a radiated wave cannot be created.

The condition for optimum extraction of energy in this case is that the radiated wave has the same frequency but opposing phase compared to the incident wave. This means that the crests of one wave coincide with the troughs of the other wave. This scenario is illustrated by the resulting superposition of the two waves on the right side of fig. 4, where the elevation of the sum of waves is smaller than that of the incident wave. The reduction of this total wave elevation is proportional to the amount of energy absorbed by the device.

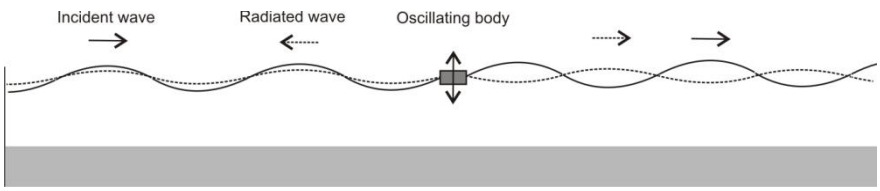

Figure 4. *Energy absorption by wave interference. The total wave field would be a sum of the radiated and incident wave (the diffracted wave field is neglected in this case). On the right side of the body the sum is less than the surface elevation of the incident wave, which means that energy has been absorbed by the body.*

The difference in phase between the incident and the radiated wave will thus be an important factor for the absorption of energy. The case of zero phase shift and equal amplitude and frequency of the radiated and incident wave would physically correspond to a body with negligible mass and damping following the incident wave exactly and therefore not generating any waves. For a realistic energy absorber the phase shift depends on the inertia and damping of the oscillating system and the geometry of the body.

Apart from the radiated wave field due to the relative displacement of the buoy, a diffracted wave field is also created, as discussed above. This is the wave field that arises when the incident wave is scattered on the surface of the body if it moves with the wave. If the dimension of the body is large, it will act as a wave breaker and the diffracted wave field will contribute to the

properties of the total wave field. On the other hand, if the body dimensions are much smaller than the incident wavelength, the diffracted wave field is negligible. This is called the point absorber-, or small body approximation (Falnes, 2002). One of the goals of this paper is to investigate if this assumption is valid when describing a wave field due to wave and body interactions for an array of point absorbers. It is the quantity $\hat{\eta}_d$ in the expression for the total wave field (16) that is subject to the small body approximation.

3.2.3 Flux of energy: an elongated body

How the absorption of energy depends on the difference in phase between incident and generated waves can be shown in the following simplified example, outlined in fig. 5. Consider an elongated body, connected to the bottom and floating on the surface, oriented perpendicular to the incident wave field. The extension of the body in the x-direction is much smaller than the incident wave length, which enables the small body approximation to be applied. The body oscillates in heave only due to the force of the incoming waves. The oscillations generate waves radiating away from each side of the body.

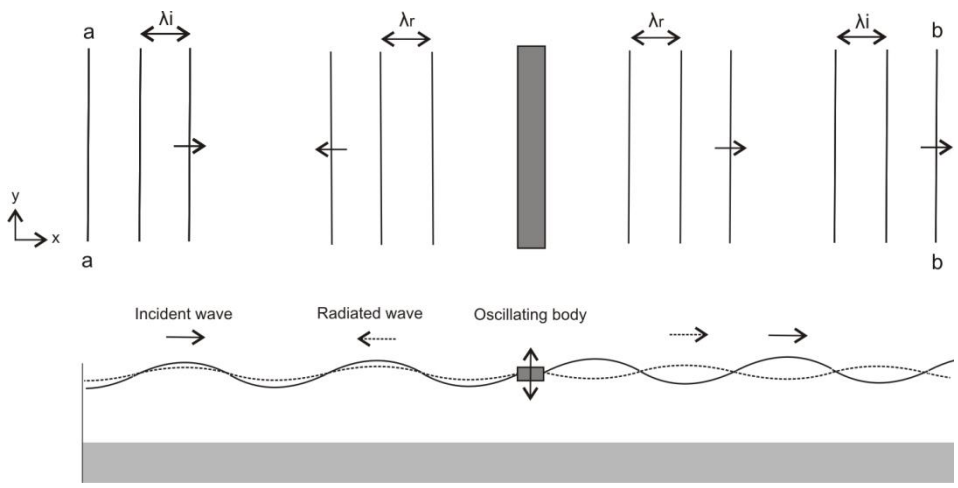

Figure 5. *Simplified case of elongated body oscillating in heave. The subscript i denotes incident wave and the subscript r denotes radiated wave. Note the positions x = a to the left and x = b to the right.*

If the perturbation pressure and the velocity are decomposed in parts due to the incident and the radiated waves, the mean energy flux per unit length of crest over one period (11) can be written as

$$\mathbb{J} = \frac{1}{T}\int_0^T \int_{-h}^0 (p_i{}' + p_r{}')(u_i + u_r)dzdt \qquad (19)$$

where the energy flux now is a vector quantity, as indicated by the bold typeface. This flux is positive for the positive x-direction. The perturbation pressure and the horizontal velocity component due to the incident waves, denoted by a subscript *i,* are given by (12) and (5). On the

left side of the body, at the position x = a, the radiated waves will propagate in the opposite direction of the incident waves. The velocity component due to the radiated wave can here be expressed as

$$u_r = -\eta_{r0}\omega \frac{\cosh\ k(z+h)}{\sinh\ kh} \cos(-kx - \omega t + \varphi) \qquad (20)$$

where η_{r0} is the amplitude of the radiated wave and φ is the phase shift between the incident and radiated waves. The contribution to the excess pressure is

$$p_r{}' = \frac{\eta_{r0}\rho\omega^2}{k} \frac{\cosh\ k(z+h)}{\sinh\ kh} \cos(-kx - \omega t + \varphi) \qquad (21)$$

The negative signs of the kx terms and the whole of (20) are caused by the negative propagation direction of the radiated wave. With the use of some algebra and the dispersion relation (6), the mean energy flux is evaluated as

$$\mathbb{J}_a = \frac{\rho g\, c_g}{8}(H^2 - 4\eta_{r0}^2) \qquad (22)$$

where the group velocity c_g is given by (8). The energy flux is not dependent on the phase shift when the waves propagate in opposite directions. For the mean energy flux to be directed towards negative x, η_{r0} would have to exceed H/2, the amplitude of the incident wave, as shown by (22).

Now consider the right side of the body in fig. 5, the position x = b. Here the whole expression for the velocity component (20) will be positive. The term –kx in the cosine argument is changed to kx, which likewise holds for the perturbation pressure (21). The resulting mean energy flux (19) now becomes

$$\mathbb{J}_b = \frac{\rho g\, c_g}{8}(H^2 + 4H\eta_{r0} cos\varphi + 4\eta_{r0}^2) \qquad (23)$$

The phase shift of the radiated wave is now one of the factors controlling the flux of energy. If there is a difference in energy flux between position b and position a, it equals the amount that is generated by the body, given by

$$\mathbb{J}_b - \mathbb{J}_a = \frac{\rho g\, c_g}{8}(4H\eta_{r0} cos\varphi + 8\eta_{r0}^2) \qquad (24)$$

A negative value of (24) means that energy has been absorbed by the body. The destructive interference is maximized as the difference in flux (24) is minimized, which occurs for a phase shift of φ = π, as given in the left panel of fig. 6. Note that this is the phase shift between the incident wave and the radiated wave and not the oscillation of the body.

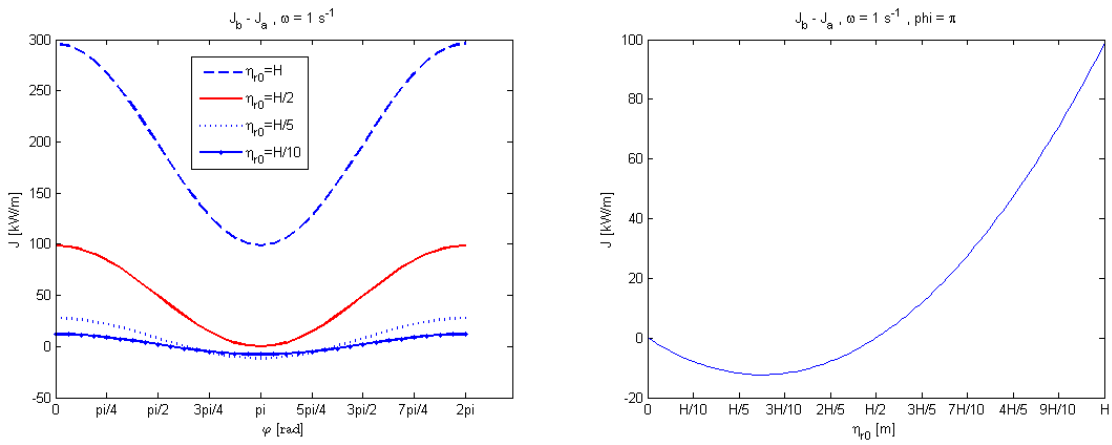

Figure 6. *The left panel shows the difference in mean energy flux for varying phase shift φ and amplitude η_{r0}. The right panel gives the difference in mean energy flux for varying amplitude η_{r0} with the phase shift φ = π. Values used are H = 2 m and ω = 1 s^{-1}.*

The right panel of fig. 6 shows how the total mean flux varies with the amplitude η_{r0} when the phase shift φ is set to π. The mean flux is minimized at a value of η_{r0} of approximately H/4. Energy is absorbed when the change in energy flux between a and b is negative. This is the case for η_{r0} less than H/2 , i.e. when the radiated wave amplitude is smaller than that of the incident wave. For the body to generate a wave with amplitude larger than the incident amplitude, an external energy source would be needed. The difference (24) increases if η_{r0} exceeds H/2, as shown by the dashed line in the left panel of fig. 6.

3.2.4 Circular waves

Consider a point absorber operating in heave only. With the small body approximation applied, only the incident and radiated waves are important. The body oscillates in heave in response to the incident wave. If the body does not exactly follow the surface of the wave, it will create a radially propagating wave, shown in fig. 7. Due to the linearity of the problem, the period of the incident and radiated waves are equal.

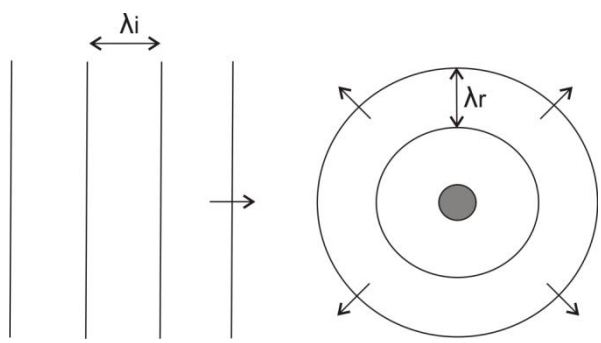

Figure 7. *An oscillating point absorber radiating circular waves in response to incident waves.*

In order to continue this discussion it is necessary to find an expression for circular propagating waves. One way to accomplish this is to solve the Laplace equation (3) for cylindrical coordinates. This leads to a Helmholz equation in the variables r and θ, which can be solved by Hankel functions. More details on this procedure are given in (Falnes, 2002). Another approach is to solve the wave equation in cylindrical coordinates (Sparr, 1999). Both solution methods give an expression for the amplitude that is proportional to $r^{-1/2}$ for r that is large compared to the wave length.

This task is greatly simplified by the use of a plane wave approximation. For large distances away from the body, the curvature of the circular radiated wave is locally small, which allows it to be approximated by a plane wave, outlined in fig. 8.

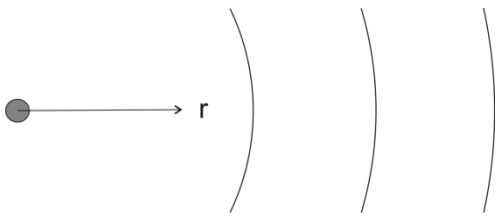

Figure 8. *Plane wave approximation. Locally, the curvature of the wave front decreases as the distance r increases.*

The condition for the plane wave approximation to be applicable is that kr >> 1 , where r is the distance away from the body and k is the wave number (McIver, 1984). However, it has been shown to be a good approximation in terms of power absorption even for values of kr approaching 1 (Mavrakos and McIver, 1997).

Using the plane wave approximation one can begin from the solution of the Laplace equation for a plane wave and modify the expression for the surface elevation (4) to be valid for a circular wave. If an ideal fluid without losses is assumed, the radiated power through a circle with radius r must be constant as the waves propagate radially with increasing r:

$$P = J2\pi r \tag{25}$$

Inserting the equation for mean energy flux (14) into (25) gives

$$P = \frac{\rho g^2 T H^2}{32\pi} 2\pi r \tag{26}$$

and from the relation between the wave height and the surface elevation (4) follows that

$$\eta \propto \frac{1}{\sqrt{r}} \ as\ r \rightarrow \infty \tag{27}$$

More strictly, it is the radiated part of the decomposed velocity potential that, besides solving the Laplace equation with boundary conditions, must fulfill a radiation condition. More details on this and the so called Sommerfeld radiation condition can be found in (Dingemans, 1997). It is convenient if the amplitude has the dimension length, so by the use of the wave number k, an expression for the surface elevation of a propagating circular wave can be written as

$$\eta_r = \frac{\eta_{r0}}{\sqrt{kr}} \cos(kr - \omega t + \varphi) \tag{28}$$

where η_{r0} is the wave amplitude and φ is the phase shift between the incident and radiated waves.

3.2.5 Flux of energy: a point absorber

To calculate the mean energy flow through a circle at the distance r from the origin, the source of the radiated wave, the perturbation pressure and the velocity are decomposed in parts due to the incident and the radiated waves as in (19). The velocity component due to the radiated circular wave, directed away from the point absorber, now reads

$$u_r = \frac{\eta_{r0}}{\sqrt{kr}} \omega \frac{\cosh\ k(z+h)}{\sinh\ kh} \cos(kr - \omega t + \varphi) \tag{29}$$

and the contribution to the excess pressure is

$$p_r{}' = \frac{\eta_{r0}}{\sqrt{kr}} \frac{\rho\omega^2}{k} \frac{\cosh\ k(z+h)}{\sinh\ kh} \cos(kr - \omega t + \varphi) \tag{30}$$

The velocity can be decomposed according to fig. 9, where x = r cos θ and y = r sin θ.

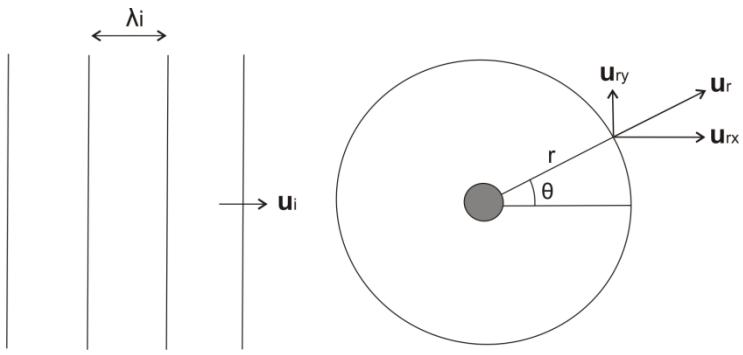

Figure 9. *Velocities due to incident and radiated waves.*

The mean energy flux per unit length of crest over one period can now be written as

$$\mathbb{J} = (\mathbb{J}_x\ ,\ \mathbb{J}_y) \tag{31}$$

where

$$\mathbb{J}_x = \frac{1}{T} \int_0^T \int_{-h}^0 (p_i{}' + p_r{}')(u_i + u_r cos\theta) dz dt \tag{32}$$

and

$$\mathbb{J}_y = \frac{1}{T} \int_0^T \int_{-h}^0 (p_i{}' + p_r{}')(u_r sin\theta) dz dt \tag{33}$$

By the use of (32), (33) and the dispersion relation, the x- and y- components can be evaluated as

$$\mathbb{J}_x = \frac{\rho g H^2 c_g}{8} + \frac{\eta_{r0}}{\sqrt{kr}} \frac{\rho g c_g}{2} \left(\frac{H}{2} cos\theta cos\psi + \frac{H}{2} cos\psi + \frac{\eta_{r0}}{\sqrt{kr}} cos\theta \right) \quad (34)$$

$$\mathbb{J}_y = \frac{\eta_{r0}}{\sqrt{kr}} \frac{\rho g c_g}{2} \left(\frac{H}{2} sin\theta cos\psi + \frac{\eta_{r0}}{\sqrt{kr}} sin\theta \right) \quad (35)$$

where the cosine argument ψ = k(rcosθ - r) - φ. To calculate the mean total power P through a circle with radius r, (31) is integrated from θ = 0 to 2π, shown in fig. 10. The positive direction of the flux is defined as outwards away from the center. Note that $\mathbb{J}$ is not necessarily directed perpendicular to the circle here.

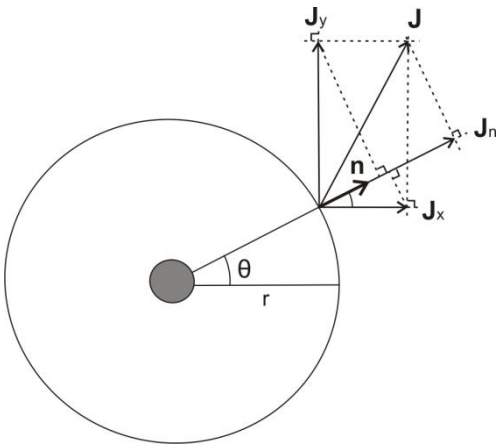

Figure 10. *Integration of the energy flux around a circle.*

The total mean power through the circle is then given by

$$P = \int_0^{2\pi} (\mathbb{J}_n \cdot \mathbb{m})\, r\, d\theta = \int_0^{2\pi} \left(\mathbb{J}_x \cos\theta + \mathbb{J}_y \sin\theta \right) r\, d\theta \quad (36)$$

which, after some manipulation, is found to be

$$P = \frac{\rho g c_g H^2}{4k} \left(\frac{\eta_{r0}\sqrt{kr}}{H} \left(\int_0^{2\pi} cos^2\theta cos\psi\, d\theta + \int_0^{2\pi} cos\theta cos\psi\, d\theta + \int_0^{2\pi} sin^2\theta cos\psi\, d\theta \right) + \frac{4\pi {\eta_{r0}}^2}{H^2} \right) \quad (37)$$

The three integrals in (37) are best solved numerically. This expression can be non-dimensionalized by dividing with $\rho g c_g H^2/4k$. Results using numerical integration are given in fig. 11. The value of the total power is minimized if the value of φ is 3π/4, as shown in the left panel of fig. 11. If the power is negative, it means that the flux is directed inwards to the body and the power is then available for absorption.

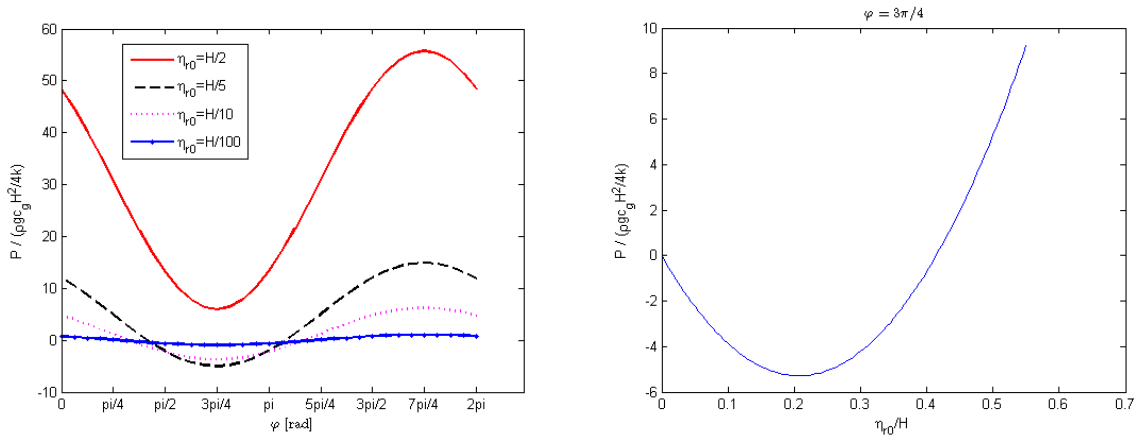

Figure 11. *The left panel shows non-dimensionalized total power for varying phase shift φ and amplitude η_{r0}. The right panel gives the same quantity for varying amplitude η_{r0} with the phase shift set to φ = 3π/4.*

The right side of fig. 11 shows how the total mean power depends on the quota η_{r0}/H when the phase shift φ is set to 3π/4. A value of η_{r0} of approximately H/5 minimizes the total mean flux in this case. The total mean power (37) can be given as

$$P = \frac{\rho g\, c_g H^2}{4k}\left(A\left(\frac{\eta_{r0}}{H}\right) + B\left(\frac{\eta_{r0}}{H}\right)^2\right) \tag{38}$$

where the sum of the integrals in A is a function of φ and B = 4π. If the radiated wave is very small compared to the wave height, $(\eta_{r0}/H)^2$ will be much smaller than η_{r0}/H. In this case the total mean power can be approximated by

$$P = \frac{\rho g\, c_g H}{4k} A\eta_{r0} \tag{39}$$

3.2.6 Wave amplitudes for an array of point absorbers

The aim of this section is to investigate how several point absorbers interact and contribute to the characteristics of the total wave field and energy content. Consider two point absorbers at position (x_1, y_1) and (x_2, y_2), placed at a distance

$$r_{12} = \sqrt{(x_2 - x_1)^2 + (y_2 - y_1)^2} \tag{40}$$

from each other, shown in fig. 12.

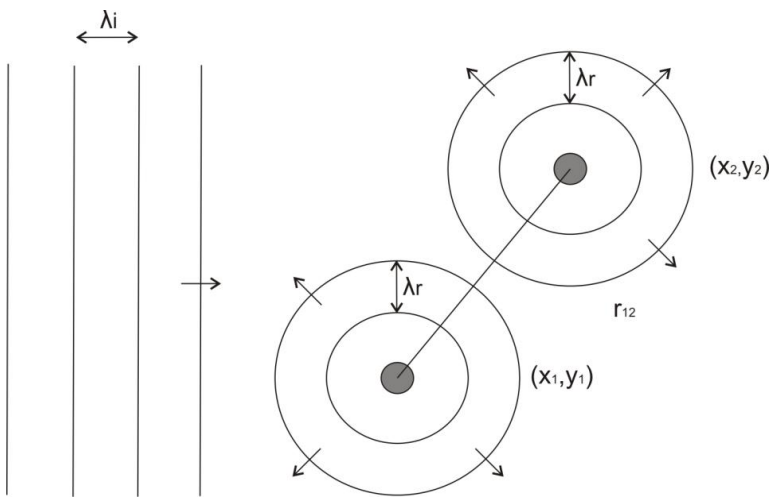

Figure 12. *Two point absorbers oscillating in response to incident and radiated waves.*

Once again both the small body- and plane wave approximations are applied. The total wave field will now depend on the incident wave and the two radiated waves, created by the oscillations of the two bodies. In describing this, a complex wave elevation $\hat{\eta}$, where

$$\eta = Re\{\hat{\eta}e^{i\omega t}\} \tag{41}$$

is the time dependent real wave elevation, is used. The surface elevation of the wave that is radiated from buoy number 1 can be written as

$$\hat{\eta}_r(r) = \hat{\eta}_i(x_1, y_1)\frac{\eta_{r0}}{\sqrt{kr}}e^{-i(kr+\varphi)} \tag{42}$$

where $\hat{\eta}_i(x_1, y_1)$ is the total incoming wave field at buoy 1 and η_{r0} is the radiated amplitude caused by an incident wave with amplitude 1 m and phase shift zero. The total wave field can be expressed with the system of two linear equations

$$\hat{\eta}_i(x_1, y_1) = \frac{H}{2}e^{-ikx_1} + \hat{\eta}_i(x_2, y_2)\frac{\eta_{r0}}{\sqrt{kr_{12}}}e^{-i(kr_{12}+\varphi)}$$

$$\hat{\eta}_i(x_2, y_2) = \frac{H}{2}e^{-ikx_2} + \hat{\eta}_i(x_1, y_1)\frac{\eta_{r0}}{\sqrt{kr_{12}}}e^{-i(kr_{12}+\varphi)} \tag{43}$$

The linear system states that the total wave elevation at position 1 is a sum of the elevation from the incident wave at position 1 and the radiated wave from position 2. This can also be expressed in matrix form as

$$\begin{bmatrix} 1 & A_{12} \\ A_{21} & 1 \end{bmatrix}\begin{bmatrix} \hat{\eta}_1 \\ \hat{\eta}_2 \end{bmatrix} = \begin{bmatrix} b_1 \\ b_2 \end{bmatrix} \tag{44}$$

$$A \qquad x \quad = b$$

where the vector b contains the incident wave elevations and the matrix A the radiated elevations. The radiated elevations are identical since r_{12} equals r_{21}. The total wave elevation at each position is then given by $x = A^{-1}b$. The linear system can be expanded to an arbitrary number of absorbers. For an array of n bodies, (44) takes the form

$$\begin{bmatrix} 1 & A_{12} & A_{13} & & \cdots & A_{1n} \\ A_{21} & 1 & A_{23} & & \cdots & A_{2n} \\ & & 1 & & & \\ \vdots & & & \ddots & & \vdots \\ & & & & 1 & \\ A_{n1} & & & & & 1 \end{bmatrix} \begin{bmatrix} \hat{\eta}_1 \\ \\ \vdots \\ \\ \hat{\eta}_n \end{bmatrix} = \begin{bmatrix} b_1 \\ \\ \vdots \\ \\ b_n \end{bmatrix} \tag{45}$$

With the use of (45), the wave elevations incident at all point absorbers in an array can be determined. It is thus possible to describe the wave field at an arbitrary position.

3.2.7 Relation between buoy movements and the radiated wave field

The generator of WEC of the Lysekil project, explained more in the next chapter, is a linear damper whose force is proportional of the velocity of the translator. The converted power is dependent on this force and the velocity according to

$$P = F_g \frac{\partial z}{\partial t} = -\gamma \left(\frac{\partial z}{\partial t}\right)^2 \tag{46}$$

where F_g is the generator force, γ is the damping coefficient and $\partial z/\partial t$ is the vertical velocity of the translator as well as the buoy. The vertical displacement of the translator and buoy can be expressed as

$$z(t) = \left|\hat{H}\right| \frac{H}{2} cos(kx - \omega t + \xi) \tag{47}$$

where $\hat{H}$ is the transfer function describing the amplitude response of the buoy to the incident wave, as described in 3.2.1, and ξ denotes the difference in phase between the motion of the buoy and the incident wave. The mean converted power over one period is

$$P = \frac{1}{T} \int_0^T \gamma \left(\frac{\partial z}{\partial t}\right)^2 dt \tag{48}$$

By using the time derivative of (47), the mean converted power can be evaluated as

$$P = \frac{1}{2} \gamma \omega^2 \left|\hat{H}\right|^2 \left(\frac{H}{2}\right)^2 \tag{49}$$

The approximation for mean power (39), derived in 3.2.5, is

$$P = \frac{\rho g\, c_g H^2}{4k} A \left(\frac{\eta_{r0}}{H}\right) \tag{50}$$

where A is a function of φ. If the deep water approximation is applied to the group velocity c_g and the wave number k in (50), the radiated amplitude η_{r0} can be given as

$$\eta_{r0} = \omega^5 \frac{H\gamma\, |\hat{H}|^2}{\rho g^3 A} \tag{51}$$

This means that the radiated amplitude is expected to be dependent on the angular frequency to the power 5.

4. Methods

The aim was to investigate how the characteristics of the wave field that arises in the interaction between heaving buoys of wave energy converters and an incoming wave influence the energy content. In order to do this, the phase shift φ between the radiated and incoming waves, as well as the amplitude of the radiated wave η_{r0} must be determined. In this context it is also interesting to test the validity of the small body approximation.

Data from the WEC of the Lysekil project (Leijon et al., 2008) was used. A model simulating a heaving point absorber connected to a viscous damper and a spring in the generator has been developed. The forces active in this model is shown on the right side of fig 13.

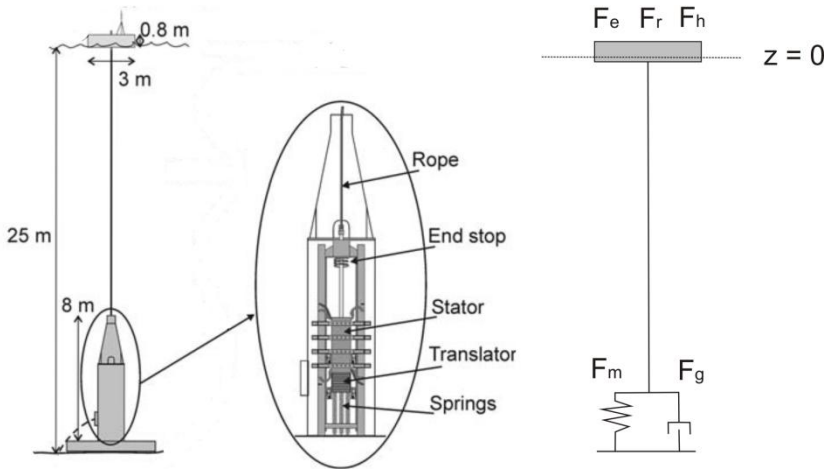

Figure 13. *Left side shows an overview of the WEC of the Lysekil project (©O.Danielsson). Right side shows the forces dominating the model simulating the system.*

The generator is modeled as a linear damper and thus the force is directly proportional to the velocity of the translator:

$$F_g = -\gamma \frac{\partial z}{\partial t} \tag{52}$$

where γ is the damping coefficient. A spring is attached to the translator acting as a restoring force. This mechanical force is proportional to the displacement of the system from its equilibrium position:

$$F_m = -k_s z \tag{53}$$

where k_s is the spring constant. The equation of motion for the whole system is

$$m\frac{\partial^2 z}{\partial t^2} = F_e + F_r + F_h + F_m + F_g \tag{54}$$

where m is the total mass of the moving parts, which are the buoy and the translator. F_e denotes the excitation force, F_r the radiation force and F_h the hydrostatic restoring force. The excitation force is the force experienced by the body if it were held fixed in its mean position in the incident wave field. The radiation force corresponds to the force upon the body due to its own

oscillations in the absence of incident waves. More details on the hydrodynamic forces are given in (Mei, 1989 and Falnes, 2002).

The radiation and excitation forces were determined using the Boundary Element Method code WAMIT. It is a three dimensional panel program that solves the radiation and excitation problems by using Green´s theorem to derive integral equations for the velocity potentials on the body boundary. For further details on solutions of boundary value problems with the use of Green´s functions, see (Newman, 1977). Data from a WEC tuned to be working efficiently in the wave climate of the Swedish west coast was used as input for WAMIT, given in table 1.

Table 1. *Data for the hydrodynamic model solved using WAMIT.*

Total moving mass	**Buoy diameter**	**Buoy draft**	**Spring constant k_s**	**Damping coeff. γ**
7037 kg	5 m	0.3 m	4 kNm^{-1}	60 $kNsm^{-1}$

The incident wave height was set to H = 2 m and calculations were carried out for five angular frequencies ω = 2, 1.5, 1, 0.75 and 0.5 s^{-1} of the incident wave. This is equivalent to the wavelengths λ = 15, 27, 62, 110 and 247 m respectively. The WEC was modeled to be centered in a field of the size 500 x 500 m with a resolution of 1 m. The WAMIT model runs were performed by Jens Engström at Uppsala University.

Results from the WAMIT runs are given as complex excited and radiated wave fields with corresponding transfer function $\widehat{H}$, described in section 3.2.1. As mentioned earlier, the terminology here differs from that used in this paper. The excited wave field WAM_{ex} is the resulting wave field if a buoy is held fixed in an incident wave field. The radiated wave field WAM_{rad} is the result of a buoy oscillating with the same phase and amplitude as the incident wave but on a surface without an incident wave. The total wave field in terms of WAMIT output is

$$\hat{\eta}_{tot} = WAM_{ex} + \widehat{H}\, WAM_{rad} \tag{55}$$

In the terminology of this paper, the diffracted wave field is the disturbance caused by a buoy moving with the same amplitude and phase as the incoming wave. In this case the total wave field can be found from (55) by setting $\widehat{H} = 1$ and the diffracted wave field is therefore

$$\hat{\eta}_d = WAM_{ex} + WAM_{rad} - \hat{\eta}_i \tag{56}$$

in which the incident wave elevation is $\hat{\eta}_i = \frac{H}{2} e^{-ikx}$. The radiated wave field is caused by the displacement of the buoy relative to the incident wave. This can be written as

$$\hat{z} - \hat{\eta}_i(0,0) = \left(\widehat{H} - 1\right)\hat{\eta}_i(0,0) \tag{57}$$

From this follows that the radiated wave field can be described as

$$\hat{\eta}_r = \left(\widehat{H} - 1\right)WAM_{rad} \tag{58}$$

Now one can see that the expression for the total wave field from section 2.2.1

$$\hat{\eta}_{tot} = \hat{\eta}_i + \hat{\eta}_d + \hat{\eta}_r \tag{59}$$

is equivalent to (55). For a small buoy, the diffracted wave field is assumed to be very small. This assumption will be tested in the next section.

5. Results

5.1 Validity of the small body approximation

Used on bodies with dimensions much smaller than the incident wavelength, the small body approximation deems the diffracted wave field negligible, implying that the quantity $\hat{\eta}_d$ can be omitted in (59). To test the validity of this assumption, the diffracted and radiated wave fields resulting from the WAMIT runs were compared. The quantity compared was the absolute value of the complex wave elevation $\hat{\eta}$, equivalent to the maximum real elevation η over one period. Mean values of the absolute value of $\hat{\eta}$ over the whole field of 500 x 500 m are given for the three incident frequencies in table 2.

Table 2. *Mean absolute value of the complex wave elevations $\hat{\eta}_r$ and $\hat{\eta}_d$ over a 500 x 500 m field for five angular frequencies of the incident wave.*

Angular frequency [s^{-1}]	**Mean radiated $\lvert \hat{\eta}_r \rvert$ [m]**	**Mean diffracted $\lvert \hat{\eta}_d \rvert$ [m]**
0.5	$2.3 \cdot 10^{-4}$	$1.4 \cdot 10^{-5}$
0.75	$2.4 \cdot 10^{-3}$	$1.7 \cdot 10^{-4}$
1	$7.1 \cdot 10^{-3}$	$4.5 \cdot 10^{-4}$
1.5	$3.1 \cdot 10^{-2}$	$2.6 \cdot 10^{-3}$
2	$3.4 \cdot 10^{-2}$	$8.0 \cdot 10^{-3}$

The results give that the mean elevation from the diffracted wave is one order of magnitude smaller that of the radiated wave. Compared with the incident wave field, with amplitude of 1 m, the diffracted wave field is at least three orders of magnitude smaller. The use of the small body approximation can thus be justified in this case.

5.2 Phase shift and amplitude of the radiated wave

The incident and radiated wave were plotted over a time series and their properties were compared. The expression for the complex surface elevation of the radiated wave (58) was used in

$$\eta_r = Re\{\hat{\eta}_r e^{i\omega t}\} \tag{60}$$

to obtain the time dependent real radiated wave. By comparing the radiated wave field

$$\eta_r = \frac{\eta_{r0}}{\sqrt{kr}}\cos(kr - \omega t + \varphi) \qquad (61)$$

along the line r = x with the incident wave, the radiated amplitude η_{r0} and the phase shift φ between the incident and radiated wave could be found. Values for x must here be sufficiently large for the plane wave approximation to be applicable. The sign of φ will be positive if there is a time lag between the moment when the body is elevated by the incident wave and the moment when the circular wave is generated by the oscillation of the body. The phase shift and radiated amplitude for the respective angular frequencies are given in table 3.

Table 3. *Phase shift φ and radiated amplitude η_{r0} for five angular frequencies of the incident wave.*

Angular frequency [s^{-1}]	**Phase shift φ [rad]**	**Amplitude η_{r0} [m]**
0.5	$0.45 \cdot 2\pi$	0.0004
0.75	$0.41 \cdot 2\pi$	0.003
1	$0.41 \cdot 2\pi$	0.01
1.5	$0.44 \cdot 2\pi$	0.08
2	$0.45 \cdot 2\pi$	0.25

There is not much difference in phase shift between the three frequencies. The mean value of φ can be approximated to 5π/6. This is a slightly higher value than the theoretical value for maximum absorption with respect to wave interference, which in section 3.2.5 was found to be 3π/4. If the angular frequency of the incident wave increases, the radiated amplitude also increases. This means that the amplitude of the circular radiated wave is proportional to the speed of the heaving oscillation of the buoy.

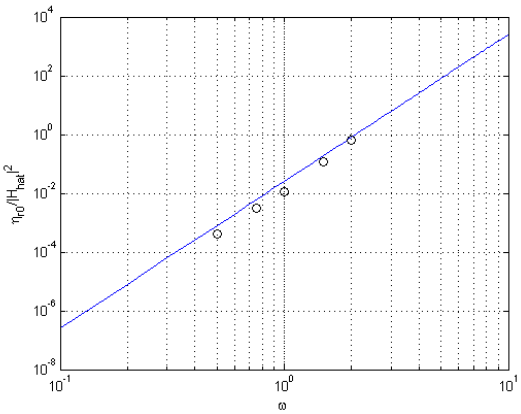

Figure 14. *Log plot of ω versus $\eta_{r0}/|\hat{H}|^2$. The line shows theoretical values according to (51) in section 3.2.7. The five circles are the values from the WAMIT runs.*

Shown in fig 14 is the quota $\eta_{r0}/|\hat{H}|^2$ for varying values of angular frequency. The conclusion of the theory in section 3.2.7 is that the radiated amplitude may be proportional to the angular frequency to the power 5. The correlation between the angle of the line, showing theoretical values from equation (51) and the circles showing the values from the WAMIT computations is good. The assumption of proportionality to the power 5 then seems reasonable. Although only five values are used here, this result supports the presented theory.

5.3 Wave field for two point absorbers

With the phase shift and radiated amplitude found with the use of the WAMIT runs, the total wave field due to the incident and radiated waves, according to the theory in section 3.2.6, could be determined. Two cases are given for a field with two point absorbers. Two different configurations of the positions, denoted (x_1, y_1) and (x_2, y_2), of the WECs are given. Firstly, in line with the incident waves and, secondly, perpendicular to the incident waves, which are coming from the left. With $\omega = 1\ s^{-1}$, the resulting wave fields on an area of 500 x 500 m for a distance r = 50 m between devices is shown in the contour plots of fig. 15. The square of the absolute value of the complex wave elevation $\hat{\eta}$, equivalent to the real amplitude, is given, since this will by (14) be proportional to the energy content. The value of kr is approximately 5 in this case, thus the condition kr >> 1 for the plane wave approximation to be applicable is fulfilled.

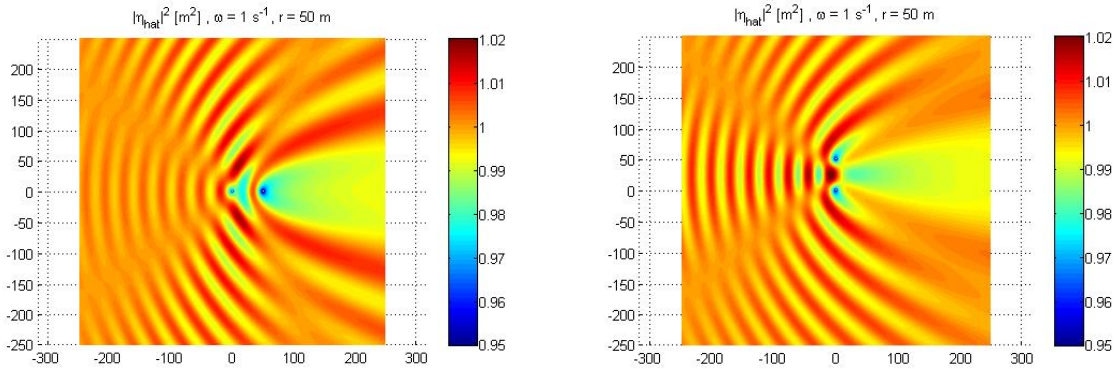

Figure 15. *Square of the amplitude for two fields with two absorbers, with the incident waves coming from the left. Device 1 positioned at (x_1, y_1)=(0,0). On the left panel, device 2 is located at (x_2, y_2)=(50,0) and on the right panel at (x_2, y_2)= (0,50), giving a distance r = 50 m in both cases. Angular frequency of the incident wave $\omega = 1\ s^{-1}$.*

As expected, the left side fig 15 shows that the amplitude is smallest on the leeside of device 2 for the in line positioning. The perpendicular positioning results in identical wave fields on the leeside of both devices, as shown by the right panel of fig. 15. The two other angular frequencies give similar wave fields, although with larger elevation for $\omega = 1.5\ s^{-1}$ and smaller for $\omega = 0.75\ s^{-1}$. If the distance r between the absorbers is varied, the resulting wave field will change. Shown in fig. 16 are the squares of the sums of the amplitudes incident at (x_1, y_1) and (x_2, y_2) for the two above configurations. This sum consists of the amplitudes of the incident wave and the radiated wave from the other device. Results are shown for varying r and incident angular frequency $\omega = 1\ s^{-1}$.

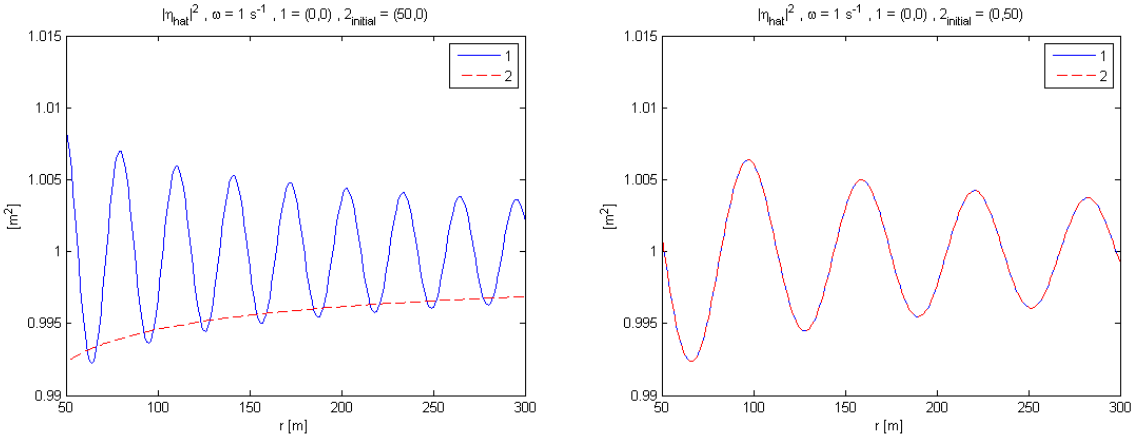

Figure 16. *Square of the total amplitude incident at (x_1, y_1)* and *(x_2, y_2) given for the two cases of configuration for varying distance between devices r. The left panel shows the in line positioning. The right panel shows the perpendicular positioning, where the amplitudes of the two waves are equal. Angular frequency of the incident wave $\omega = 1\ s^{-1}$.*

As seen in fig. 16, the variation of the amplitude for device number 1 in the in line configuration , shown to the left, oscillates with a frequency approximately 2 times higher than the amplitude of both devices for the perpendicular configuration, shown to the right. By the linearity of the problem, the amplitudes for the two other frequencies also follow this pattern of oscillations. For the perpendicular configuration, amplitudes for both devices are equal for all r. The incident wave length is 62 m in this case. Low values are experienced when r is equal to approximately a multiple of the wave length. This can be explained by the phase shift $\varphi = 5\pi/6$ between the incident and the radiated wave. The radiated wave is almost in counter phase with the incident wave and thus the destructive interference is largest for these values. The reverse is true for values of r equal to a multiple of half the wave length, where high wave elevation values occur due to positive destruction. As r goes to infinity, both amplitudes tend to one for each of the two cases.

5.4 Wave field for arrays of point absorbers

For wave energy conversion using point absorbers to be profitable, several converters must be employed in a whole farm. The total energy absorption of the whole farm is then an important factor to optimize. First an example of an array with 7 WECs is given. The devices are arranged in a regular staggered grid of three rows, made up of 6 equilateral triangles, shown in fig. 17.

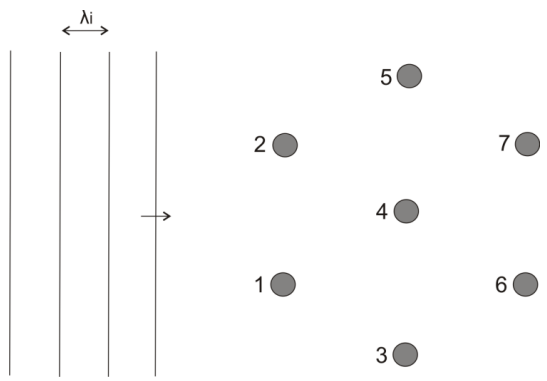

Figure 17. *Regular staggered grid with 7 WECs.*

Each row of absorbers remove power from the waves and thus there is less power left on the leeside. The absorption by the first row results in less power available for consecutive rows. But this does not change the fact that the distance between devices can be set to maximize the amplitude of the wave field with respect to wave interference. In this case there are 7 radiated waves interacting with the incident wave. The linear system of section 3.2.6 now contains 7 equations. The resulting wave field for an area of 500 x 500 m for a distance r = 50 m between devices is shown in the contour plot of fig. 18

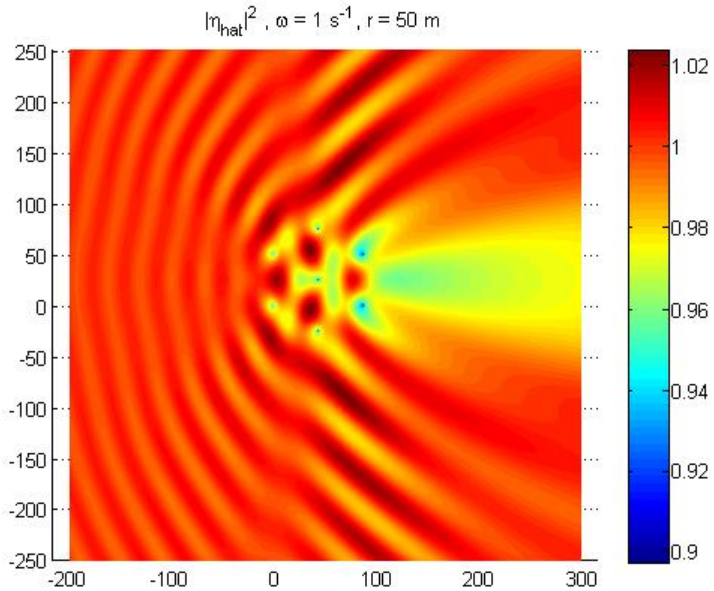

Figure 18. *Square of the amplitude for a field with an array of 7 absorbers, with the incident wave coming from the left. The distance between devices r = 50 m.*

In a small area on the leeside of the array, the square of the amplitude is approximately 0.95. This is by (14) equal to a loss of 5 % of the incident wave energy. If the angular frequency of the incident wave is set to $\omega = 0.75$ and 1.5 s^{-1}, this ratio will be approximately 2 % and 15 % respectively. To judge the effect of the variation of the distance between devices on the whole array, the mean of the square of the amplitudes incident at all of the 7 devices, is given in fig. 19 for varying r. The amplitude at (x_1, y_1) is a sum of the amplitudes of the incident wave and the 6 radiated waves from the other devices. A mean is then taken for this wave amplitude at the 7 different positions, given for varying r.

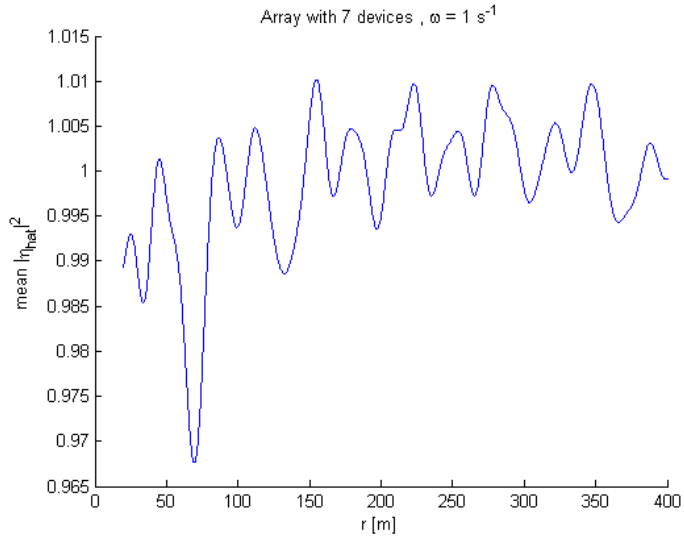

Figure 19. *Mean of square of the amplitudes incident at all devices, for an array with 7 devices at varying distance between devices r. Angular frequency of the incident wave ω = 1 s^{-1}.*

Figure 19 shows that the lowest and highest values are approximately 0.97 and 1.01. This amounts to a difference in mean energy content of 4 % of the wave field incident at the devices. Figures for ω = 0.75 and 1.5 s^{-1} are 1 and 30 % respectively. Significantly contributing to this difference are the low values experienced when the ratio between the distance and the incident wave length r/λ is approximately 1.1. In fig. 19 this occurs at a distance r = 69 m, since the wave length is 62 m in this case. This can, as discussed in the preceding chapter, be attributed to the phase shift, which equals 5π/6.

To apply the computations on a realistic case, the grid is now expanded to an array of 420 WECs, approximately the size of the farm planned by the company Seabased to be located outside of Smögen. The grid, again composed of equilateral triangles, consists of 12 rows with 35 devices in each row, oriented perpendicular to the incident waves, shown in fig. 20.

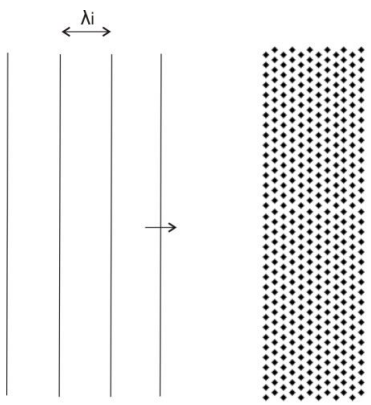

Figure 20. *Regular staggered grid with 420 WECs.*

Using a distance r = 50 m between devices, the dimensions of the grid is approximately 500 x 1700 m, giving an area of about 0.8 km^2. The linear system of 420 equations is solved and the resulting wave field is shown in the contour plot of fig. 21, with incident frequency ω = 1 s^{-1}.

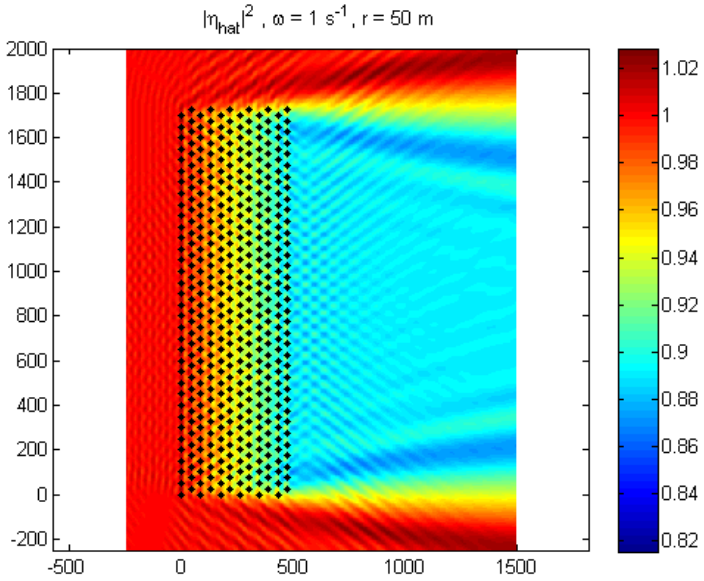

Figure 21. *Square of the amplitude for a field with an array of 420 absorbers, with the incident wave coming from the left. The distance between devices r = 50 m.*

In the whole area on the leeside of the farm, the square of the amplitude is reduced to approximately 0.9. This is equal to a loss of 10 % in energy content due to the whole farm. For a lower angular frequency, this loss will be less significant and vice versa. The frequency $\omega = 1\ s^{-1}$ is close to the value that will contribute the largest amount of energy transport on a yearly basis at the site outside of Smögen (Waters et al., 2009). The variation of the wave elevation for different r, just as in the example with 7 devices but this time for 420 devices, is given in fig. 22. Mean values of the square of the maximal wave elevations incident at all devices are shown here.

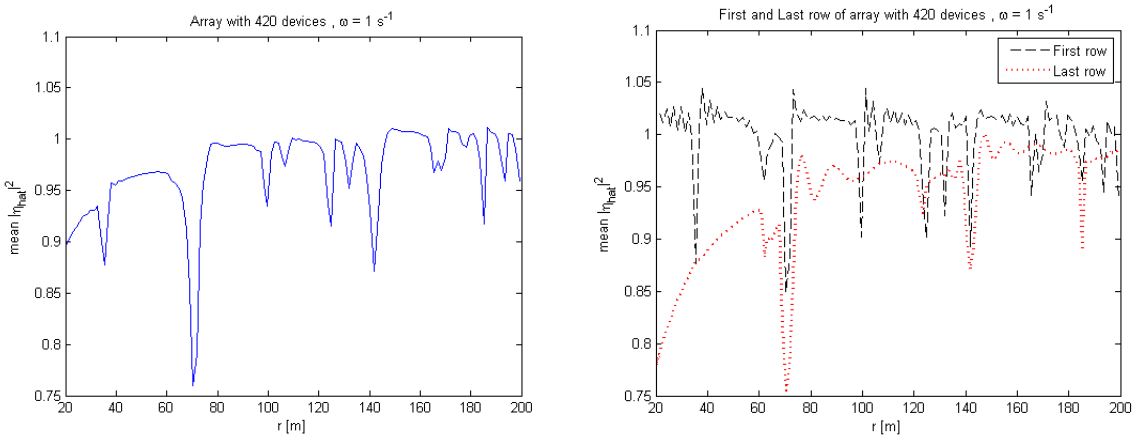

Figure 22. *Mean of square of the amplitudes incident at all devices for an array with 420 devices at varying distance between devices r shown in the left panel. The right panel shows mean of square of the amplitude incident at the devices of the first and last row of the array. Angular frequency of the incident wave $\omega = 1\ s^{-1}$.*

The highest value 1.01 occurs at the distance r = 187 m, while the lowest value 0.76 is for r = 70 m. For the lowest value, both the first and last row experiences their minima. This difference in wave elevation corresponds to a difference in energy content of 25 % at the waves that are

incident at the devices. The minimum value occurs for all three frequencies when the ratio r/λ is approximately 1.1, just as in the preceding example with 7 devices.

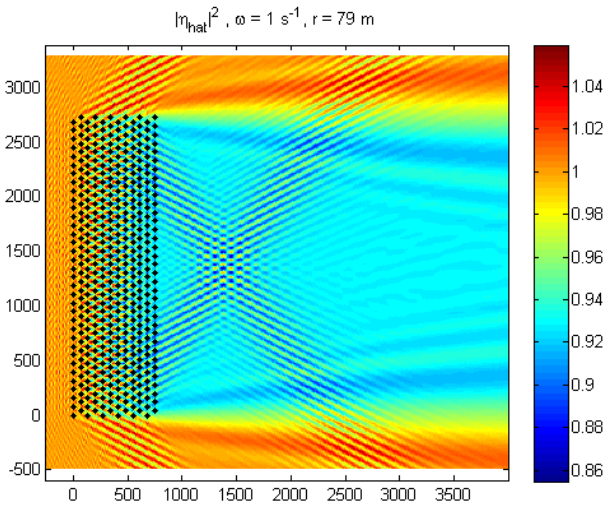

Figure 23. *Square of the amplitude for a field with an array of 420 absorbers, with the incident wave coming from the left. The distance between devices r = 79 m.*

In the contour plot of fig. 23, another example of a wave field is shown. The distance between devices is now 79 m, for which a high mean value occurs according to fig. 22. The square of the amplitude is this time reduced to approximately 0.93, equivalent to an energy loss of 7 %. A larger area around the array is plotted which reveal some interesting effects in the wave field, such as the X-shape to the right of the farm. It is unfortunately beyond the scope of this paper to interpret such phenomena. If there is a large distance between the farm and the coastline, there is greater possibility for the wind to put more energy into the waves, and thus make up for the loss due to the wave farm. From an environmental aspect this would be positive, but the costs of transferring the electricity to the shore would be higher.

6. Discussion and conclusions

Methods to describe the effects on the wave field due to interaction effects between the oscillating buoys of wave energy converters have been developed in this paper. The influence of the phase shift between the radiated waves and the incident wave on these effects has been shown. Further important factors found were the amplitude of the radiated wave, as well as the distance between the devices employed in an array. With the use of these methods, a model describing the wave field at an arbitrary position in an area surrounding an array of wave energy converters was developed. The results could be useful when assessing the impact of a wave energy farm on the marine and benthic environment. The reduction of energy in the wave field may lead to changes in the area surrounding the farm as well as the coastline. For a location with energetic seas and a high rate of sediment transport, a modification of energy levels could possibly have large effects.

A large part of the papers cited in this thesis regard the subject of enhancement or optimization of the energy absorption of WECs. In this complex task, aimed at single devices or arrays of

devices, several control parameters and restrictions must be considered. The results in this paper indicate that the constructive or destructive interference of wave amplitudes at different spacing of an array may be a parameter to consider. The difference in the wave energy incident at all the devices of a large array due to different spacing distances could be significant. Applying a typical frequency at a real location to the case of the array with 420 devices of the Lysekil project type, choosing an inappropriate spacing distance could possibly correspond to a substantial loss of power. A conclusion is that a distance between devices that is the same as a typical wave length is probably best avoided, if a system with the same characteristics as the one discussed in this paper is to be used.

A relevant question is how well hydrodynamic models using linear wave theory describe the behavior of wave energy absorbers in the real ocean. (De Beule et al., 2009) performed laboratory tests to validate the modeling of point absorbers with linear theory both in the time and frequency domain. It was concluded that that the linear theory models are in good accordance with experimental results regarding power absorption. Modeled results from the Lysekil system using linear theory were compared with experimental data from a prototype WEC by (Eriksson et al., 2007). The results show that the linear model is well suited to simulate wave-buoy interactions.

In this paper the body motion is restricted to only one degree of freedom, which is heave. This approximation is probably realistic, since the interactions between the heave mode and the other modes are very small (Falcão et al., 2007 and Falnes, 2002). The small body- or point absorber approximation was found to be justifiable. Other authors have reached the same conclusion in circumstances with long waves and wide spacing between devices (Mavrakos and McIver, 1997 and Ricci et al., 2007). The plane wave approximation gives good agreement with more exact methods, provided the large spacing condition is not violated, as shown by (Mavrakos and McIver, 1997 and McIver, 1984).

One way to improve the findings in this paper would be to apply the computations to polychromatic and irregular waves. This could possibly give a more realistic description of how different spacing between the devices influence energy content.

7. Acknowledgments

I would like to thank my supervisor Lars Arneborg for putting up with me a second time. Fortunately my multitude of not always well defined questions the last time did not put you off so I could again share your knowledge of the ocean. Many thanks also for all the Matlab tricks. A second time thank you also goes to my associate supervisor Jens Engström. Your insight of wave energy research has really improved my efforts. Kai Christensen of the Norwegian Meteorological Institute is thanked for discussions on waves in general and the possible direction of this paper in particular. Johan Karlsson of the mathematics department of GU is acknowledged for advice regarding analysis. Christian Stranne is thanked for help with numerics. Also thank you Lars Tornberg of Chalmers for input on wave solutions.

8. References

Caracas M C (2003) The OPD Pelamis WEC: Current status and onward programme. *International Journal of Ambient Energy*, *vol. 24, 2003*.

Cruz J (2008) Ocean Wave Energy. *Springer*, Berlin Heidelberg, Germany.

Cruz J, Sykes R, Siddorn P, Eatock Taylor R (2009) Wave Farm Design: Preliminary Studies on the Influences of Wave Climate, Array Layout and Farm Control. *Proceedings of the 8th European Wave and Tidal Energy Conference,* Uppsala, Sweden.

De Backer G, Vantorre M, Beels C, De Rouck J (2009) Performance of closely spaced point absorbers with constrained floater motion. *Proceedings of the 8th European Wave and Tidal Energy Conference,* Uppsala, Sweden.

De Beule K, De Backer G, Vantorre M, Beels C, De Rouck J (2009) Experimental investigation of the validity of linear theory to assess the behaviour of a heaving point absorber at the Belgian continental shelf. *Proceedings of the 28th International Conference on Ocean, Offshore and Arctic Engineering*, Hawaii, USA.

Dingemans M W (1997) Water wave propagation over uneven bottoms. Part 1 – Linear wave propagation. Advanced Series on Ocean Engineering-vol. 13. *World Scientific*, Singapore.

Engström J (2009) Hydrodynamic Modeling of the Energy Conversion from Ocean Waves to Electricity. *Licentiate Thesis*, Uppsala University, Sweden.

Engström J, Eriksson M, Isberg J, Leijon M (2009) A Wave Energy Converter with enhanced amplitude response at frequencies coinciding with Swedish west coast sea states by use of supplementary added mass. *Journal of Applied Physics 106.*

Engström J, Waters R, Stålberg M, Strömstedt E, Eriksson M, Isberg J, Henfridsson U, Bergman K, Asmussen J, Leijon M (2007) Offshore experiments on a direct-driven Wave Energy Converter. *Proceedings of the 7th European Wave and tidal Energy conference,* Porto, Portugal.

Eriksson M, Waters R, Svensson O, Isberg J, Leijon M (2007) Wave power absorption: Experiments in open sea and simulation. *Journal of Applied Physics 102*.

Falcão A F de O (2000) The shoreline OWC wave power plant at the Azores. *Proc 4th Eur Wave Power Conf, paper B1.* University of Aalborg, Denmark.

Falcão A F de O, Saulnier J B, Ricci P, Pontes M T (2007) Time-Domain models and wave energy converters performance assessment. *Proceedings of the 7th European Wave and Tidal Energy conference,* Porto, Portugal.

Falnes J (2002) Ocean waves and oscillating systems, linear interaction including wave-energy extraction. *Cambridge University press*, Cambridge, United Kingdom.

Fitzgerald C, Thomas G (2007) A preliminary study on the optimal formation of an array of wave power devices. *Proceedings of the 7th European Wave and Tidal Energy conference,* Porto, Portugal.

Holthuijsen L H (2007) Waves in oceanic and coastal waters. *Cambridge University Press,* Cambridge, United Kingdom.

Isberg J, Eriksson M, Leijon M (2008) Transport of energy in polychromatic fluid gravity waves. *Journal of Engineering Mathematics 64, pp 15-23*.

Kalén O (2009) Exploring the influence of a wave energy farm on the wave induced bottom friction on the Swedish west coast. *Bachelor Thesis.* University of Gothenburg, Sweden.

Kofoed J P, Frigaard P, Friis-Madsen E, Sørensen H C (2006) Prototype testing of the wave energy converter Wave Dragon. *Renewable energy*, *31:181–189*.

Kundu P K (2008) Fluid Mechanics. *Academic Press Inc*., San Diego, USA.

Leijon M, Boström C, Danielsson O, Gustafsson S, Haikonen K, Langhamer O, Strömstedt E, Stålberg M, Sundberg J, Svensson O, Tyrberg S, Waters R (2008) Wave Energy from the North Sea: Experiences from the Lysekil Research Site. *Surveys in Geophysics, volume 29, pp 221–240.*

Linton C M, McIver P (2001) Mathematical Techniques for Wave/Structure Interactions. *Chapman and Hall/CRC*. Boca Raton, Florida, USA.

Mavrakos S A, McIver P (1997) Comparison of methods for computing hydrodynamic characteristics of arrays of wave power devices. *Applied Ocean Research, 19:283–291.*

McIver P (2002) Wave interaction with arrays of structures. *Applied Ocean Research 24, 121–126*

McIver P (1984) Wave forces on arrays of bodies. *Journal of Engineering and Mathematics, 18:273–285.*

Mei C C (1989) The Applied Dynamics of Ocean Surface Waves. *World Scientific Publishing*, Singapore, 1983. Second printing.

Newman J N (1977) Marine Hydrodynamics. *MIT Press,* Cambridge, USA.

Ricci P, Saulnier J B, Falcão A F de O (2007) Point-absorber arrays: a configuration study off the Portuguese West-Coast. *Proceedings of the 7th European Wave and tidal Energy conference,* Porto, Portugal.

Saulnier J B, Ricci P, Falcão A F de O, Pontes M T (2007) Sensitivity of an axisymmetrical wave energy converter to spectral bandwidth. *Proceedings of the 7th European Wave and Tidal Energy conference,* Porto, Portugal.

Sparr G, Sparr A (1999) Kontinuerliga System. *Studentlitteratur,* Lund, Sweden.

Wamit user manual: http://www.wamit.com/manual.htm.

Waters R, Engström J, Isberg J, Leijon M (2009) Wave climate off the Swedish west coast. *Renewable Energy 34, pp. 1600-1606.*

Yilmaz O, Incecik A (1998) Analytical solutions of the diffraction problem of a group of truncated vertical cylinders. *Ocean Engineering 1998; 25:385–94.*